Supplementary Material

A peanut shell-derived economical and eco-friendly biochar catalyst for electrochemical ammonia synthesis under ambient conditions: combined experimental and theoretical study

Anmin Liu [a,*], Yanan Yang [a], Xuefeng Ren [b,*], Mengfan Gao [a], Xingyou Liang [a], Tingli Ma [c,d,*]

[a] State Key Laboratory of Fine Chemicals, School of Chemical Engineering, Dalian University of Technology, China.

E-mail: anmin0127@163.com, liuanmin@dlut.edu.cn

[b] School of Ocean Science and Technology, Dalian University of Technology, Panjin, 124221, China.

E-mail: renxuefeng@dlut.edu.cn

[c] Department of Materials Science and Engineering, China Jiliang University, Hangzhou, 310018, China.

[d] Graduate School of Life Science and Systems Engineering, Kyushu Institute of Technology, 2-4 Hibikino, Wakamatsu, Kitakyushu, Fukuoka 808-0196, Japan.

E-mail: tinglima@life.kyutech.ac.jp

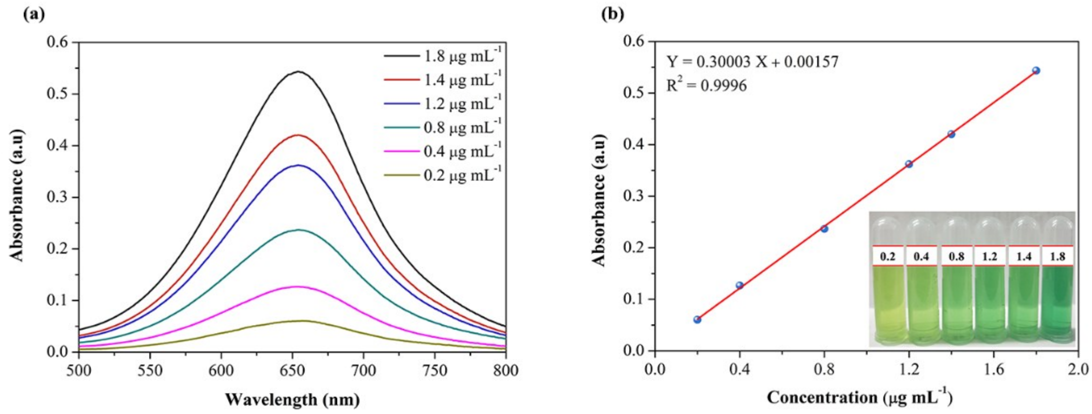

Fig. S1. (a) UV-vis spectra for NH_4^+ standard solutions with different concentrations, (b) the calibration curve for NH_4^+ quantification.

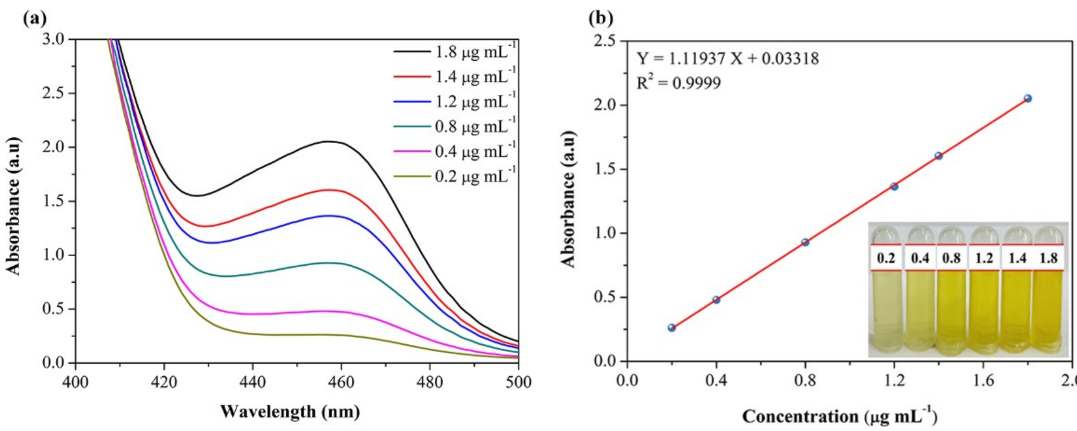

Fig. S2. (a) UV-vis spectra for N_2H_4 standard solutions with different concentrations, (b) the calibration curve for N_2H_4 quantification.

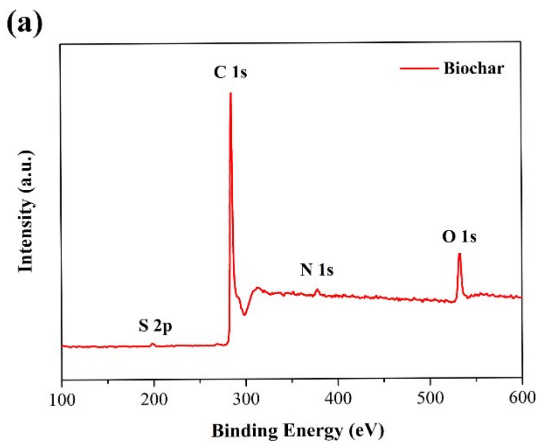

Fig. S3. XPS survey of biochar catalyst (a) before reaction, (b) after reaction.

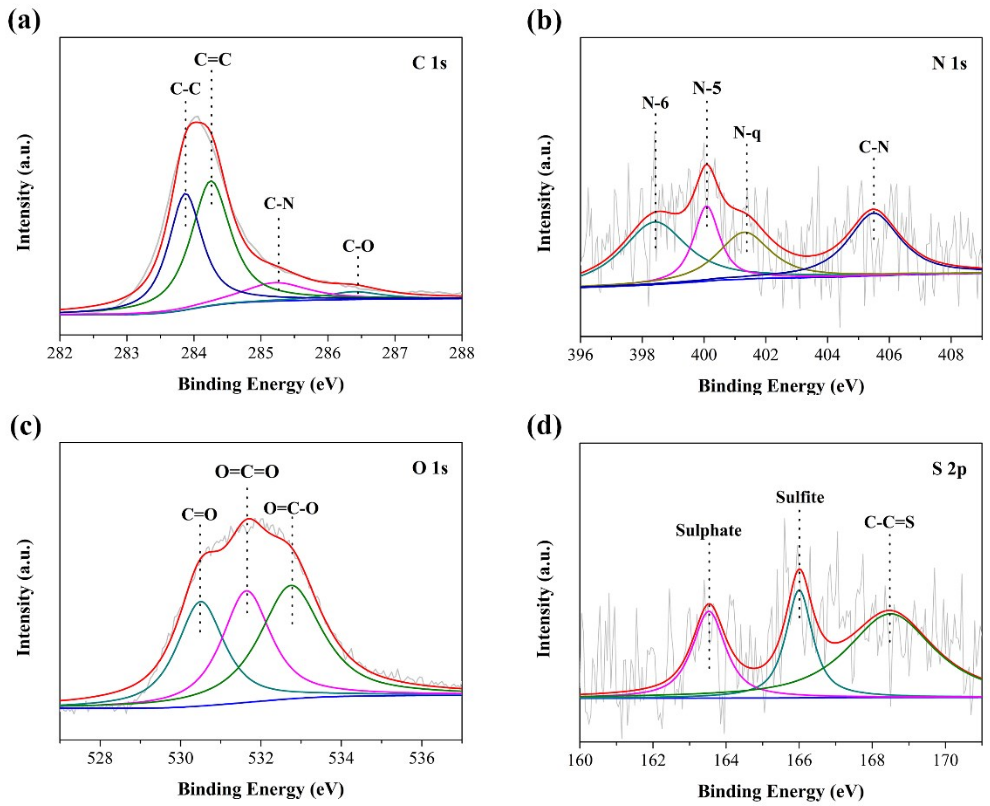

Fig. S4. High resolution XPS spectra of (a) C 1s, (b) N 1s, (c) O 1s, and (d) S 2p of the biochar catalysts after rection.

Table. S1. The percentage of each element in the biochar catalyst before and after the reaction.

Species \ Elements	C 1s	N 1s	O 1s	S 2p	K 2p
Before	88.41	1.43	9.22	0.34	0.61
After	92.02	0.66	5.03	0.13	2.17

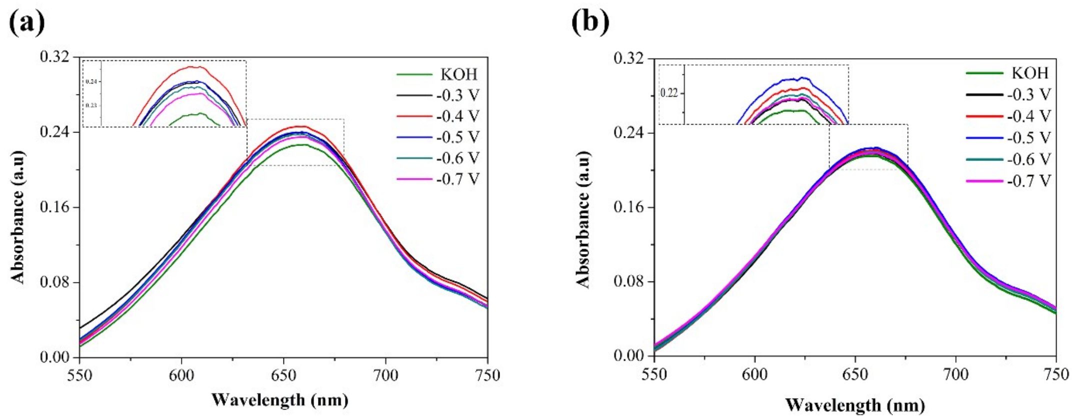

Fig. S5. UV-visible spectra of the electrolyte stained by indophenol blue indicator after 2 h of reduction reaction in N_2 saturated 0.1 M KOH at various potential. (a) biochar ,(b) graphite.

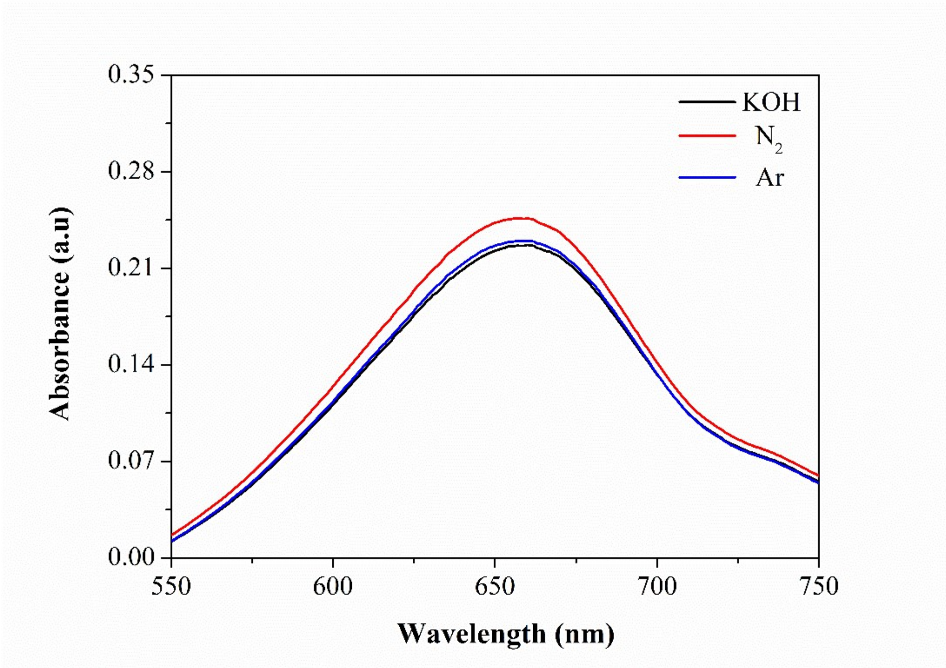

Fig. S6. UV-visible test of the electrolyte after reaction at -0.4 V *vs.* RHE.

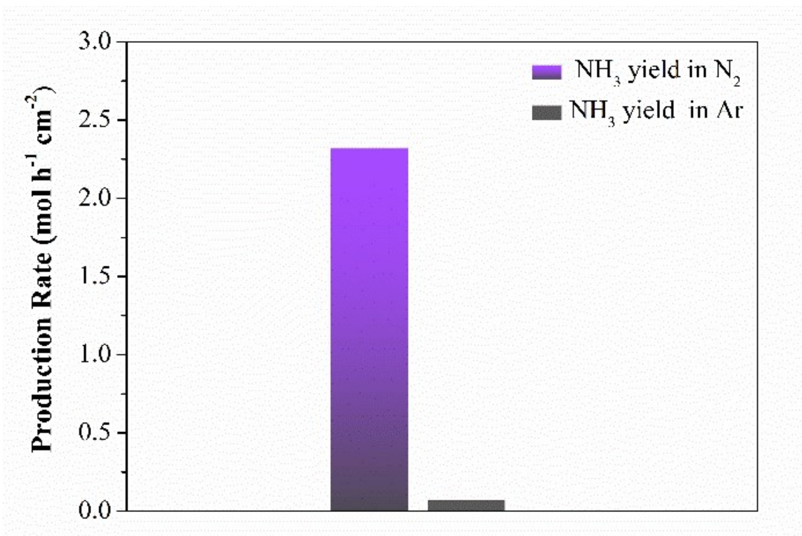

Fig. S7. Ammonia yield in N_2 and Ar environments at -0.4 V *vs.* RHE potential.

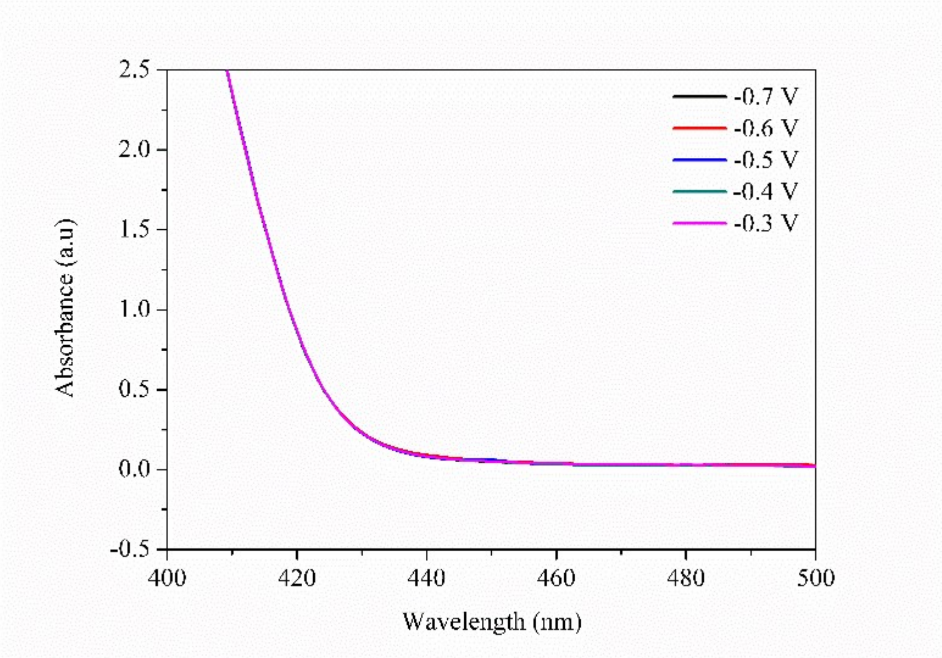

Fig. S8. UV-visible test of N_2H_4 of electrolytes after different potentials.

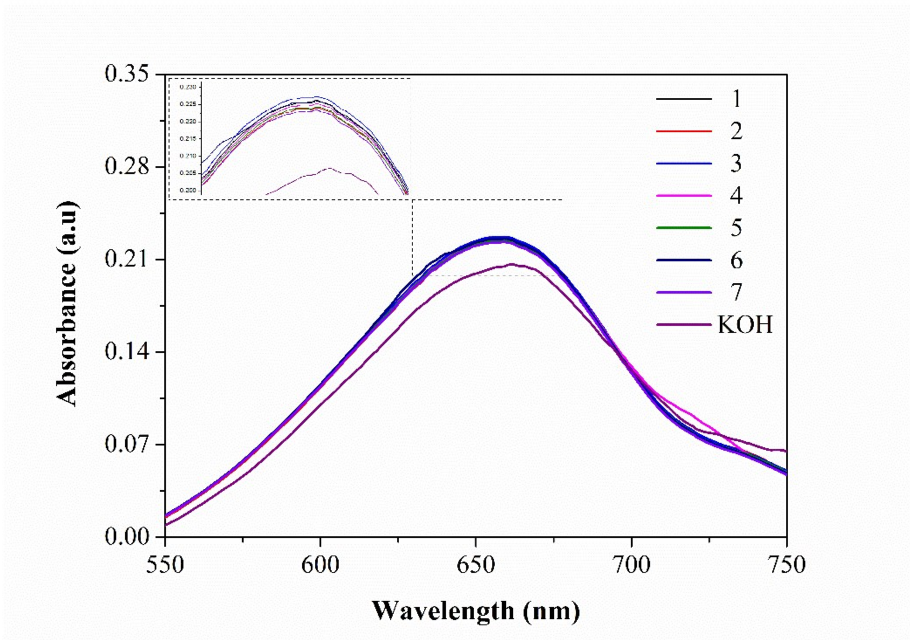

Fig. S9. UV-visible test of 7 cycles of reaction at -0.4 V *vs.* RHE potential.

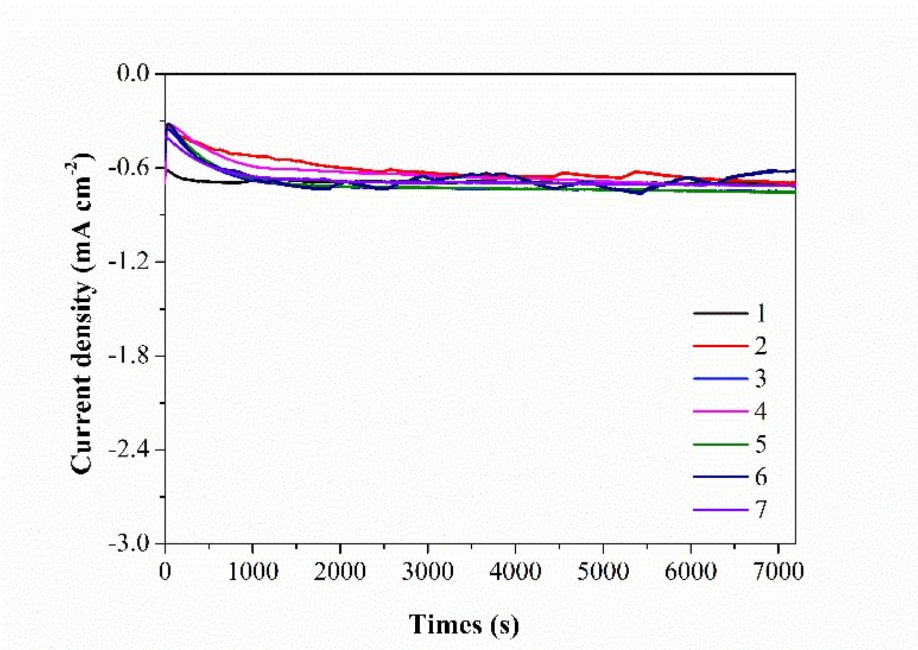

Fig. S10. i - t curves of 7 cycles of reaction at a potential of -0.4 V *vs.* RHE.

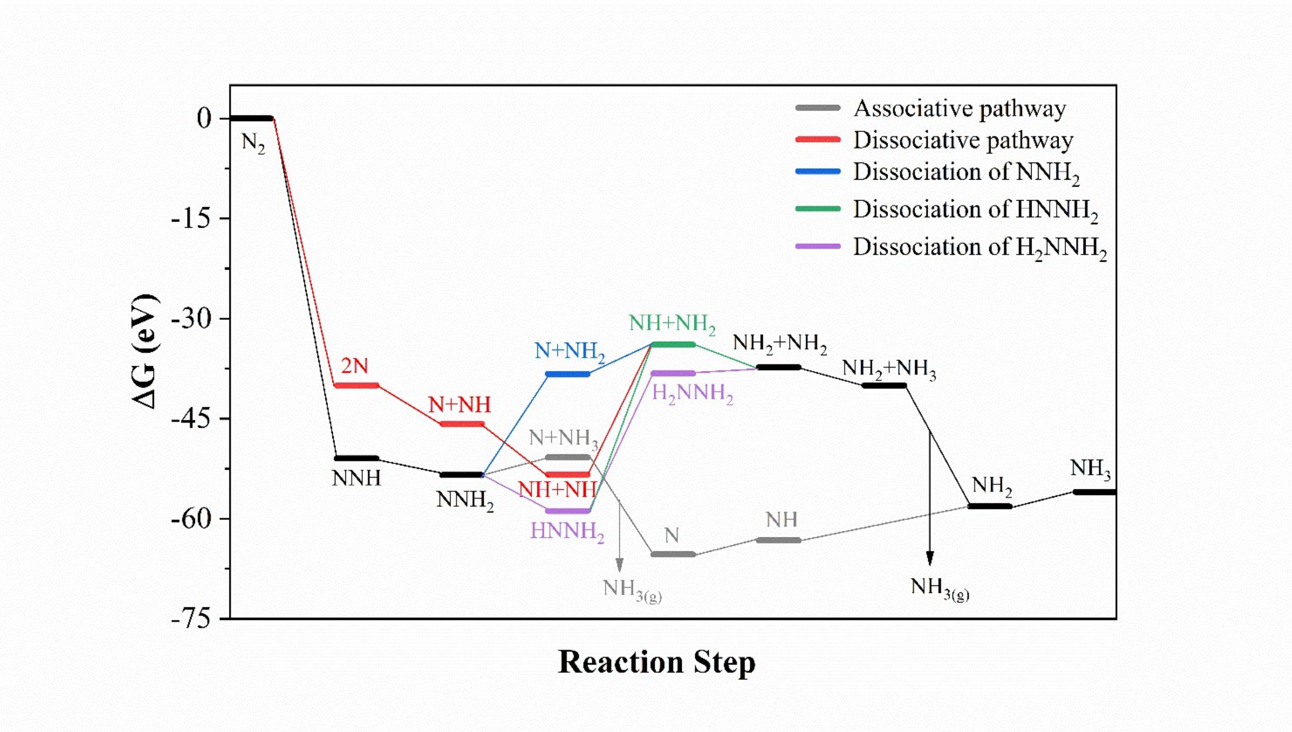

Fig. S11 Free energy diagrams of NRR at the peanut shell-derived biochar with Bio-O37 as active site.

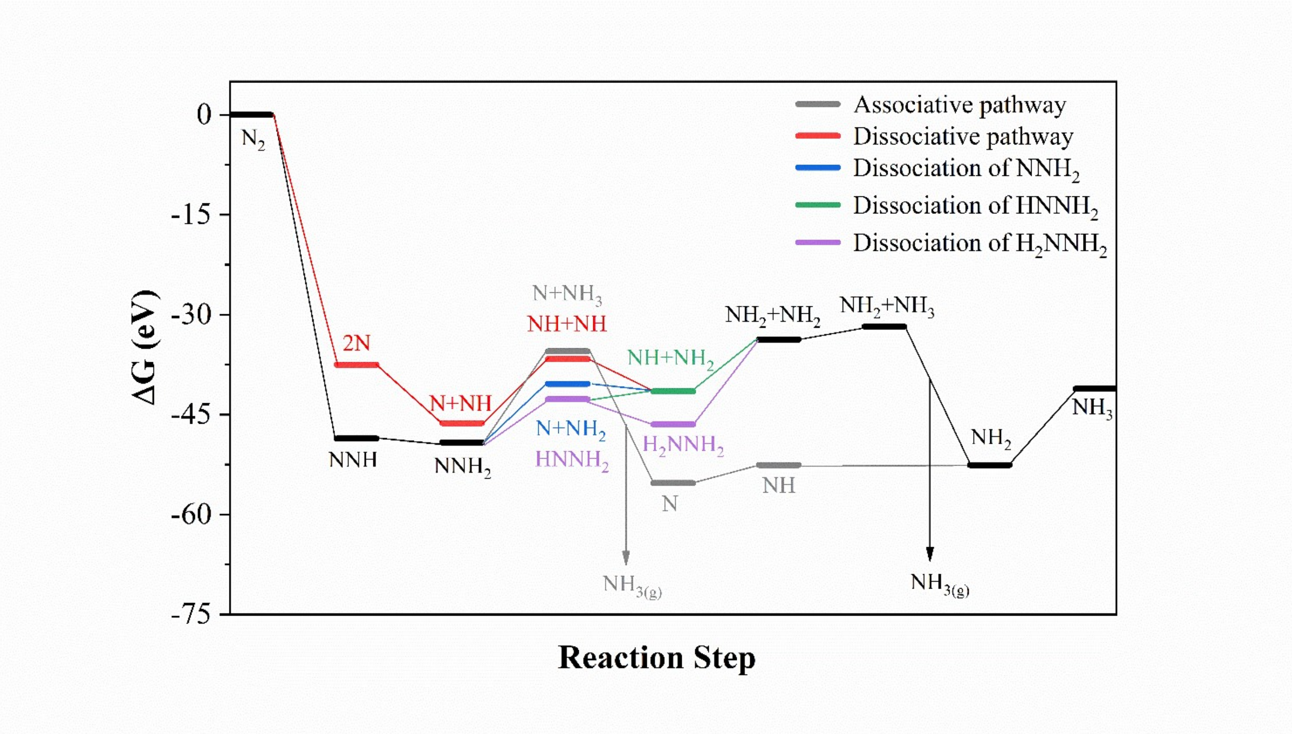

Fig. S12 Free energy diagrams of NRR at the peanut shell-derived biochar with Bio-O15 as active site.

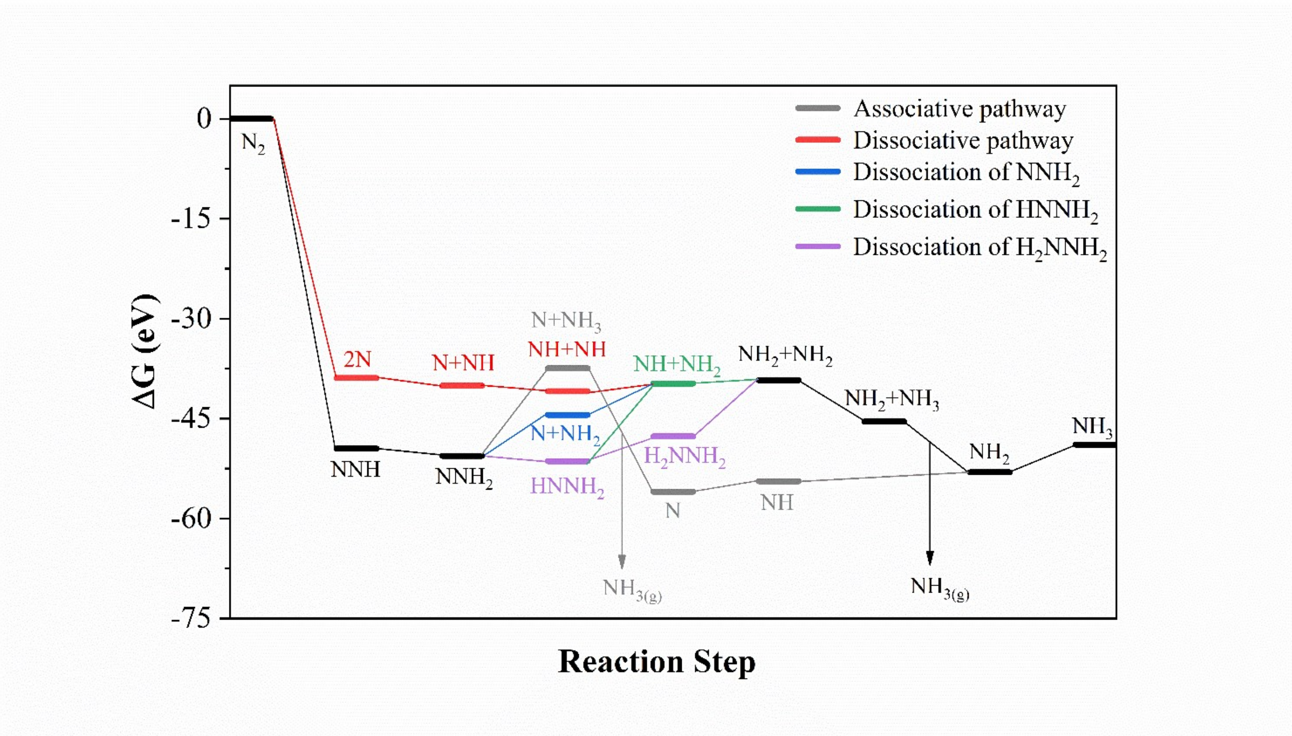

Fig. S13 Free energy diagrams of NRR at the peanut shell-derived biochar with Bio-O21 as active site.

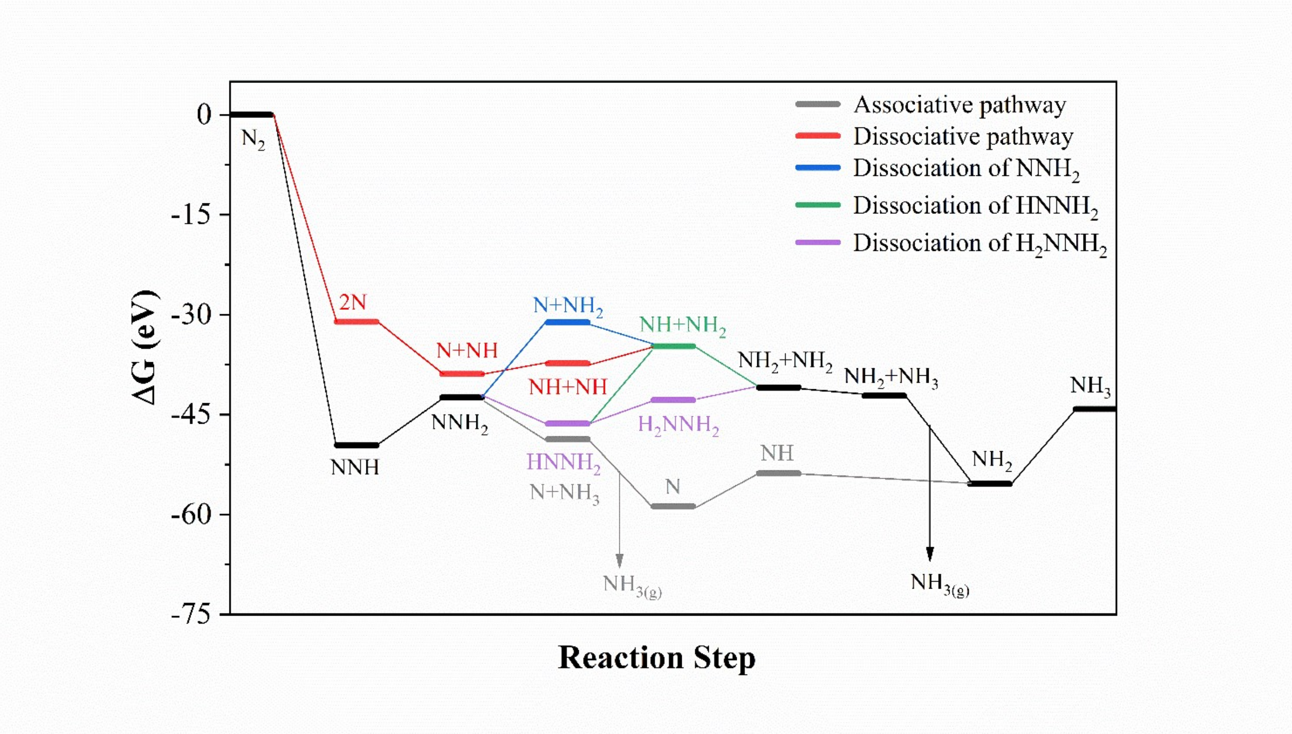

Fig. S14 Free energy diagrams of NRR at the peanut shell-derived biochar with Bio-O37 as active site.

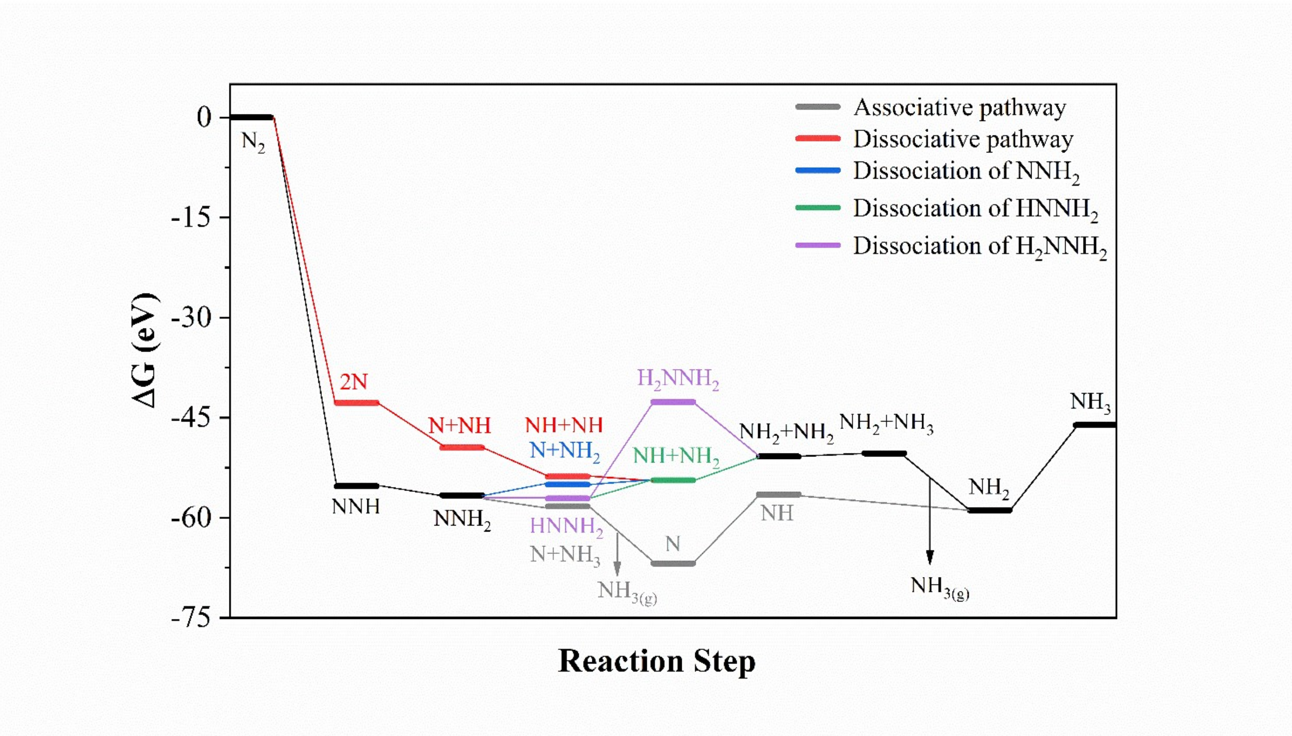

Fig. S15 Free energy diagrams of NRR at the peanut shell-derived biochar with Bio-S58 as active site.

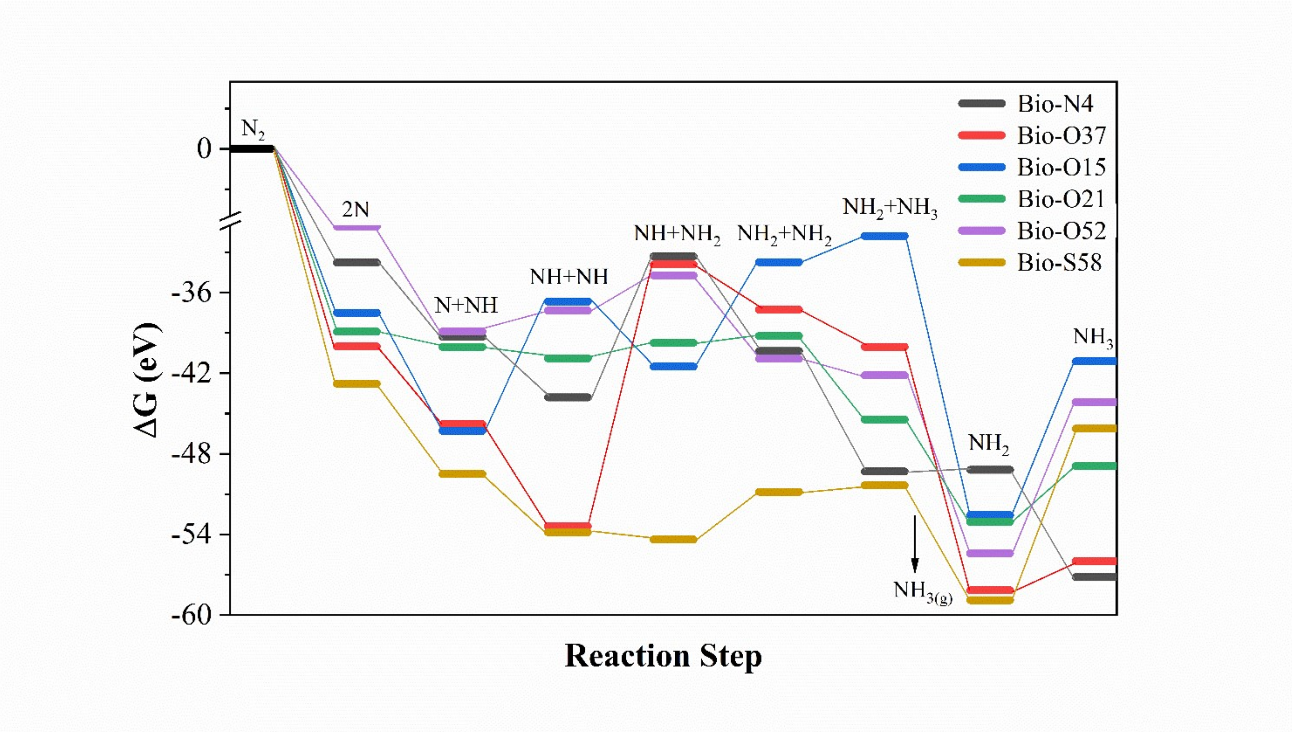

Fig. S16 Free energy diagrams of NRR for Dissociative pathway on these six biochar active sites of Bio-N4, Bio-O37, Bio-O15, Bio-O21, Bio-O52, and Bio-S58.

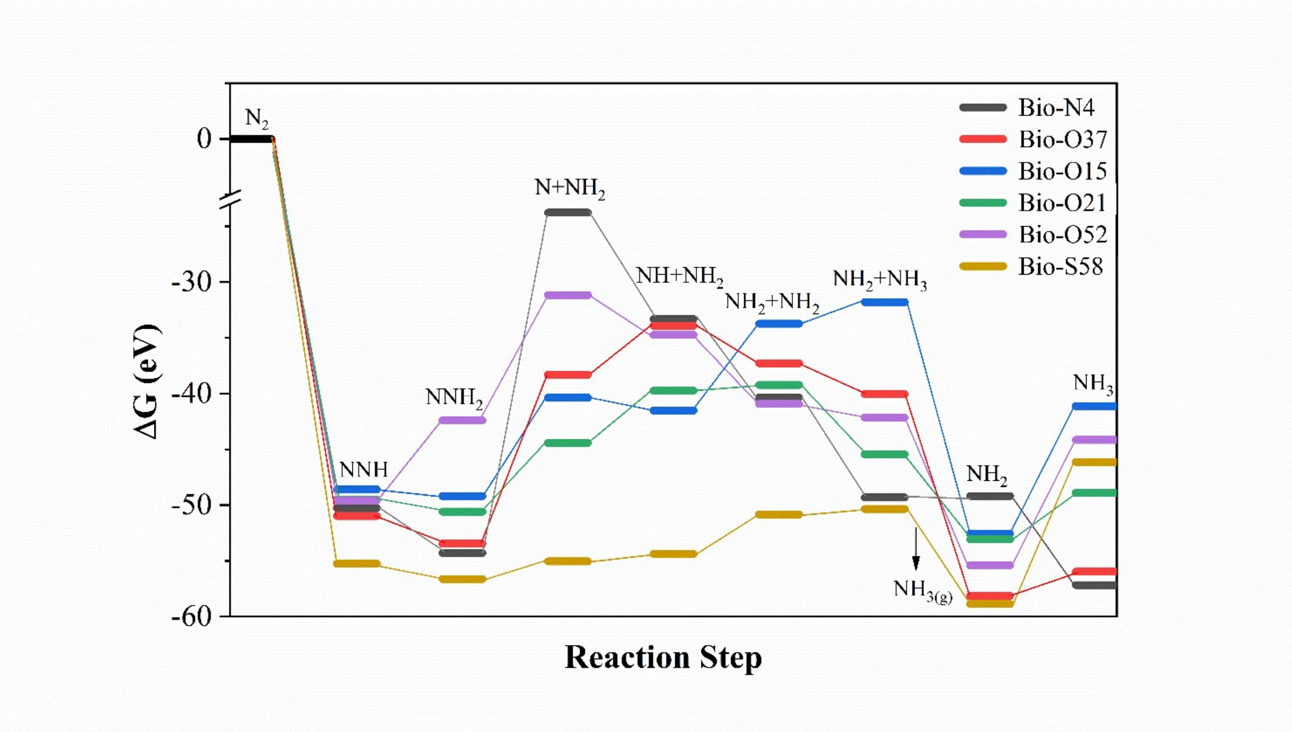

Fig. S17 Free energy diagrams of NRR for Dissociation of NNH_2 on these six biochar active sites of Bio-N4, Bio-O37, Bio-O15, Bio-O21, Bio-O52, and Bio-S58.

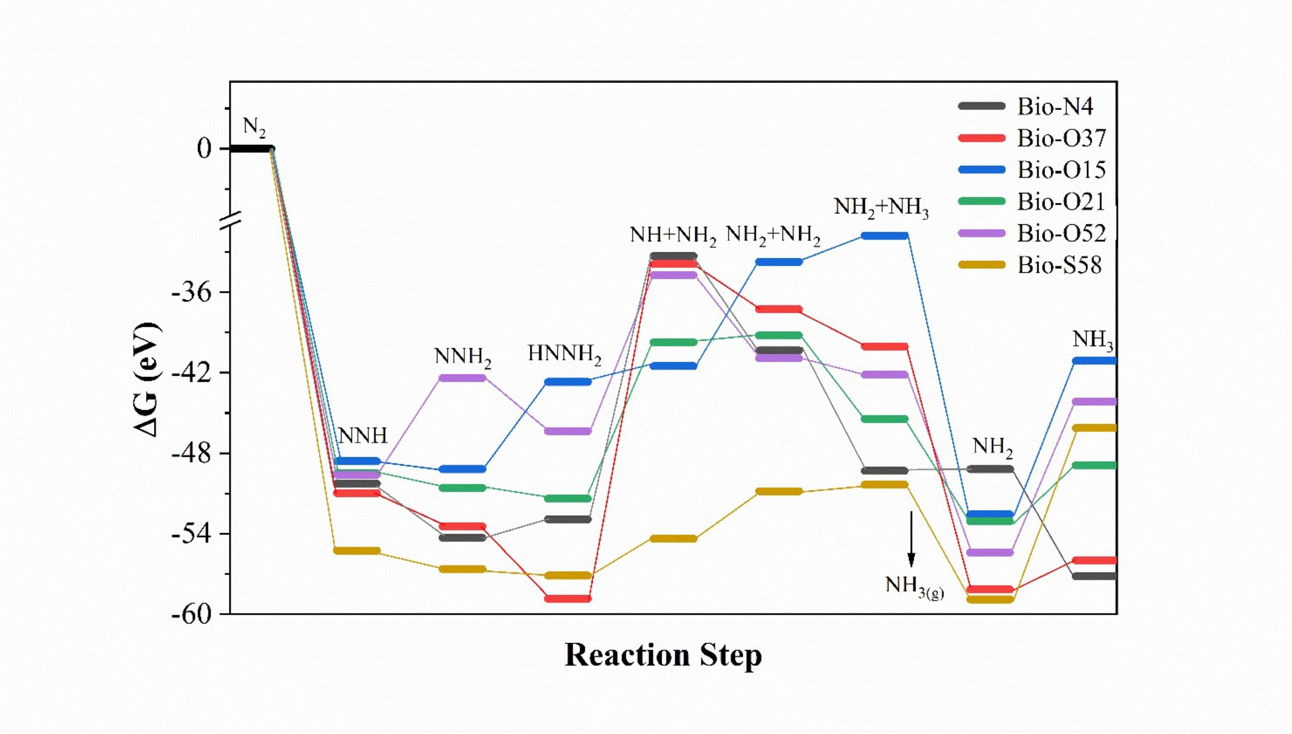

Fig. S18 Free energy diagrams of NRR for Dissociation of $HNNH_2$ on these six biochar active sites of Bio-N4, Bio-O37, Bio-O15, Bio-O21, Bio-O52, and Bio-S58.

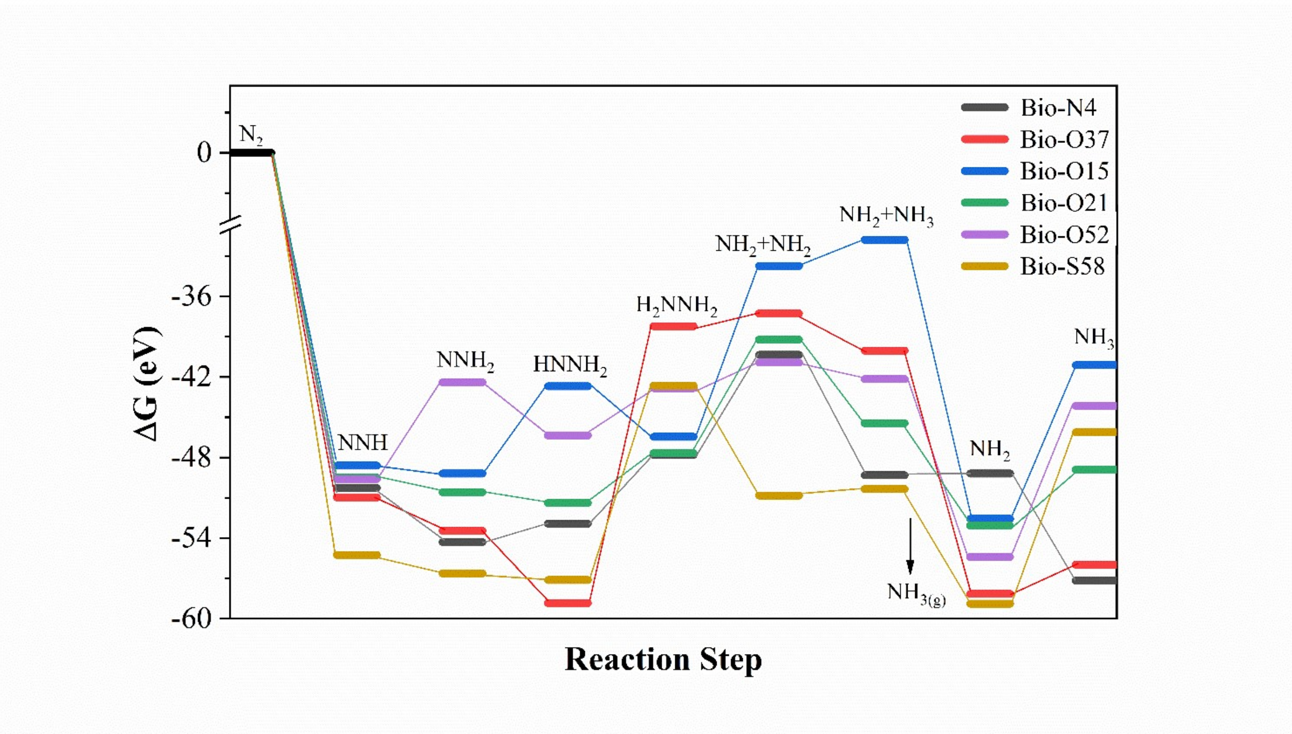

Fig. S19 Free energy diagrams of NRR for Dissocition of H_2NNH_2 on these six biochar active sites of Bio-N4, Bio-O37, Bio-O15, Bio-O21, Bio-O52, and Bio-S58.

Carbon species	Source	Preparation conditions	Reaction conditions	Reaction potential	Ammonia yield	FE (%)	Ref.
N-doped porous carbon	ZIF-8	N_2; 1100℃; 1 h	0.1 M KOH	-0.3 V *vs.* RHE	3.4×10^{-6} mol cm^{-2} h^{-1}	10.2	[1][1]
	ZIF-8	H_2/N_2; 750℃; 5 h	0.05 M H_2SO_4	-0.9 V *vs.* RHE	6.0×10^{-7} mol cm^{-2} h^{-1}	1.5	[2][2]
	ZIF-67	N_2; 500℃; 3 h Air; 250℃; 10 h	0.05 M H_2SO_4	-0.2 V *vs.* RHE	42.58×10^{-6} g h^{-1} $mg^{-1}_{cat.}$	8.5	[3][3]
Fe-N/C-CNTs	$(CH_3COO)_2Fe$; Multiwall carbon nanotubes; ZIF-8	N_2; 1000℃; 1 h	0.1 M KOH	-0.2 V *vs.* RHE	34.83×10^{-6} g h^{-1} $mg^{-1}_{cat.}$	9.28	[4][4]
Carbon nanotubes	Fe_2O_3; Carbon nanotubes	350℃; 2 h	$KHCO_3$	-2.0 V *vs.* Ag/AgCl	1.3×10^{-8} mol cm^{-2} h^{-1}	0.15	[5][5]
	Carbon nanotubes	HNO_3；80℃；24 h	0.1 M $LiClO_4$	-0.4 V *vs.* RHE	33.23×10^{-6} g h^{-1} $mg^{-1}_{cat.}$	12.5	[6][6]
Polymeric carbon nitride	Melamine	Ar; 550°C; 4 h Ar; 620°C; 4 h	0.1 M $LiClO_4$	-0.2 V *vs.* RHE	8.09×10^{-6} g h^{-1} $mg^{-1}_{cat.}$	11.59	[7][7]
B-doped graphene	H_3BO_3 ; Graphene oxide	H_2/Ar; 900℃;3 h	0.05 M H_2SO_4	-0.5 V *vs.* RHE	5.76×10^{-7} g h^{-1} $mg^{-1}_{cat.}$	10.8	[8][8]
Graphene oxide	$PdCl_2$; $CuCl_2$; Graphene oxide	Ar; stirring for 2 h	0.1 M KOH	-0.2 V *vs.* RHE	2.80×10^{-6} g h^{-1} $mg^{-1}_{cat.}$	4.5 (0.0 V vs RHE)	[9][9]
	$CeCl_3\cdot7H_2O$; Graphene oxide	Hydrothermal; 160℃; 24 h	0.1 M Na_2SO_4	-0.7 V *vs.* RHE	16.98×10^{-6} g h^{-1} $mg^{-1}_{cat.}$	4.78	[10][10]
	Na_2CrO_4; Graphene oxide	Hydrothermal; 150℃; 24 h Ar; 700°C; 1 h	0.1 M HCl	-0.7 V *vs.* RHE	33.3×10^{-6} g h^{-1} $mg^{-1}_{cat.}$	7.33 (−0.6 V vs RHE)	[11][11]
S-doped carbon Nanospheres	Glucose; Benzyl disulfide	180℃; 10 h Ar; 800℃; 2 h	0.1 M Na_2SO_4	-0.7 V *vs.* RHE	19.07×10^{-6} g h^{-1} $mg^{-1}_{cat.}$	7.47	[12][12]
Sulfur dots – graphene	Graphite rods; Na_2SO_4; Na_2S	Electrochemical process	0.5 M $LiClO_4$	-0.85 V *vs.* RHE	28.56×10^{-6} g h^{-1} $mg^{-1}_{cat.}$	7.07	[13][13]
Biochar	Peanut shells	N_2; 1100℃; 1 h	0.1 M KOH	-0.4 V *vs.* RHE	2.32×10^{-6} mol h^{-1} cm^{-2} 或 39.81×10^{-6} g h^{-1} $mg^{-1}_{cat.}$	26.97	This work

Reference

1. S. Mukherjee, D. A. Cullen, S. Karakalos, K. Liu, H. Zhang, S. Zhao, H. Xu, K. L. More, G. Wang and G. Wu, *Nano Energy,* 2018, **48**, 217-226

2. Yanming Liu, Yan Su, Xie Quan, Xinfei Fan, Shuo Chen, Hongtao Yu, Huimin Zhao, Yaobin Zhang and J. Zhao, *ACS Catal.,* 2018, **8**, 1186-1191

3. S. Luo, X. Li, B. Zhang, Z. Luo and M. Luo, *ACS App.l Mater. Interfaces,* 2019, **11**, 26891-26897

4. Y. Wang, X. Cui, J. Zhao, G. Jia, L. Gu, Q. Zhang, L. Meng, Z. Shi, L. Zheng, C. Wang, Z. Zhang and W. Zheng, *ACS Catal.,* 2018, **9**, 336-344

5. S. Chen, S. Perathoner, C. Ampelli, C. Mebrahtu, D. Su and G. Centi, *Angew. Chem. Int. Edit.,* 2017, **56**, 2699-2703

6. J. Zhao, B. Wang, Q. Zhou, H. Wang, X. Li, H. Chen, Q. Wei, D. Wu, Y. Luo, J. You, F. F. Gong and X. Sun, *Chem. Commun.,* 2019, **55**, 4997-5000

7. C. Lv, Y. Qian, C. Yan, Y. Ding, Y. Liu, G. Chen and G. Yu, *Angew. Chem. Int. Edit.,* 2018, **57**, 10246-10250

8. X. Yu, P. Han, Z. Wei, L. Huang, Z. Gu, S. Peng, J. Ma and G. Zheng, *Joule,* 2018, **2**, 1610-1622

9. M.-M. Shi, D. Bao, S.-J. Li, B.-R. Wulan, J.-M. Yan and Q. Jiang, *Adv. Energy Mater.,* 2018, **8**, 1800124

10. H. Xie, Q. Geng, X. Li, T. Wang, Y. Luo, A. A. Alshehri, K. A. Alzahrani, B. Li, Z. Wang and J. Mao, *Chem. Commun.,* 2019, **55**, 10717-10720

11. L. Xia, B. Li, Y. Zhang, R. Zhang, L. Ji, H. Chen, G. Cui, H. Zheng, X. Sun, F. Xie and Q. Liu, *Inorg. Chem.,* 2019, **58**, 2257-2260

12. L. Xia, X. Wu, Y. Wang, Z. Niu, Q. Liu, T. Li, X. Shi, A. M. Asiri and X. Sun, *Small Methods,* 2018, **3**, 1800251

13. H. Chen, X. Zhu, H. Huang, H. Wang, T. Wang, R. Zhao, H. Zheng, A. M. Asiri, Y. Luo and X. Sun, *Chem. Commun.,* 2019, **55**, 3152-3155